Nonadiabatic effects on surfaces: Kohn anomaly, electronic damping of adsorbate vibrations, and local heating of single molecules



2008 J. Phys.: Condens. Matter 20 224015

(http://iopscience.iop.org/0953-8984/20/22/224015)

IOP PUBLISHING JOURNAL OF PHYSICS: CONDENSED MATTER

J. Phys.: Condens. Matter **20** (2008) 224015 (9pp) doi:10.1088/0953-8984/20/22/224015

# Nonadiabatic effects on surfaces: Kohn anomaly, electronic damping of adsorbate vibrations, and local heating of single molecules

**J Kröger**

Institut für Experimentelle und Angewandte Physik, Christian-Albrechts-Universität zu Kiel, D-24098 Kiel, Germany

E-mail: kroeger@physik.uni-kiel.de

Received 8 November 2007, in final form 28 November 2007
Published 13 May 2008
Online at stacks.iop.org/JPhysCM/20/224015

**Abstract**

Three aspects of electron–phonon coupling at metal surfaces are reviewed. One aspect is the Kohn effect, which describes an anomalous dispersion relation of surface phonons due to quasi-one-dimensional nesting of Fermi surface contours. The combination of electron energy loss spectroscopy and angle-resolved photoelectron spectroscopy allows us to unambiguously characterize Kohn anomaly systems. A second aspect is the nonadiabatic damping of adsorbate vibrations. Characteristic spectroscopic line shapes of vibrational modes allow us to estimate the amount of energy transfer between the vibrational mode and electron–hole pairs. Case studies of a Kohn anomaly and nonadiabatic damping are provided by the hydrogen- and deuterium-covered Mo(110) surface. As a third aspect of interaction between electrons and phonons, local heating of a $C_{60}$ molecule adsorbed on Cu(100) and in contact with the tip of a scanning tunnelling microscope is covered.

(Some figures in this article are in colour only in the electronic version)

## 1. Introduction

The interaction between vibrational and electronic degrees of freedom at metal surfaces is at the origin of some macroscopic effects. An example is the heat capacity of metals, to which electrons contribute according to $\gamma T$, where $T$ denotes the temperature and $\gamma$ describes the enhancement of the electron band mass at the Fermi level due to electron–phonon coupling [1, 2]. Probably the most famous example for electron–phonon coupling is provided by conventional superconductivity. The interaction between electrons and phonons below a critical temperature leads to an attractive interaction of electrons resulting in the formation of Cooper pairs [3].

Much work has been devoted to measuring the electron–phonon coupling parameter which characterizes the strength of the interaction between electrons and phonons. The above mentioned heat capacity and the transition temperature of conventional superconductors depend on this parameter. Photoemission experiments have access to the electron–phonon coupling parameter by monitoring the temperature dependence of the width of a photoemission peak [4–14], by determining renormalized bands at the Fermi level [15–18], or by extracting the Eliashberg coupling function from the measured self-energy [19]. In the case of Kohn anomaly systems the temperature dependence of the anomaly was exploited to obtain the electron–phonon coupling strength [20]. For a survey of measured electron–phonon coupling parameters and the techniques involved the reader is referred to [21].

Besides the electron–electron coupling, the electron–phonon interaction is among the fundamental interactions in solids. A detailed understanding of these interactions is crucial in the field of nanoscale physics, where quantum size effects are important and these interactions will inevitably affect the decay rates of excited hole or electron states. For instance, decay rates of electron excitations play an important role in surface chemistry, where a reaction often proceeds via an

 

intermediate electronically excited state. A pertinent question is then whether the lifetime of the excited state is compatible with the time it takes for the reactants to complete the reaction. Hellsing *et al* [22] reported on theoretical approaches to include lattice vibrations in determining the decay rate of electronic excitations. In a review article by Echenique *et al* [23], experimental and theoretical decay rate data were compared.

In this article, the focus is on Kohn anomaly systems (section 3), on the nonadiabatic electronic damping of adsorbate vibration modes (section 4), and on the local heating of a single molecule in contact with the tip of a scanning tunnelling microscope (section 5).

## 2. Experiment

The presented data were acquired in ultra-high vacuum with base pressures ranging from $10^{-9}$ to $10^{-8}$ Pa. Molybdenum surfaces were cleaned by repeated oxygen annealing cycles and intermediate heating of the samples close to their melting temperature. For copper surfaces several argon ion bombardment and annealing cycles were performed. Atomic hydrogen and deuterium were adsorbed on Mo(110) by exposing the surface to $H_2$ and $D_2$ gas of 99.995% purity. Fullerene molecules were evaporated from a tantalum crucible and deposited on Cu(100) at room temperature. Chemically etched tungsten wire served as tip material for the scanning tunnelling microscopy experiments. *In vacuo*, the tip was annealed, subsequently bombarded with argon ions and gently indented into the copper substrate.

Vibrational spectra were measured by electron energy loss spectroscopy (EELS) using a custom-built spectrometer operated with an energy resolution of 1.5 meV [24] and an angle resolution of better than 1° (corresponding to a wavevector resolution of better than 0.04 $\text{Å}^{-1}$ for the applied impact electron energies). The resolution characteristics correspond to the full width at half maximum (FWHM). Phonons with different wavevectors $\mathbf{q}_\parallel$ parallel to the surface were measured by rotating the analyser of the spectrometer so as to capture electrons which transferred a momentum of $\mathbf{q}_\parallel$.

Angle-resolved photoelectron spectroscopy (ARPES) experiments were carried out in a modified Vacuum Generators Escalab 220 spectrometer [25]. For ultraviolet photoemission, He I$\alpha$ radiation (21.2 eV) was used and the pass energy of the hemispherical analyser was set so as to obtain an energy resolution of 35 meV FWHM. The angle resolution was less than 1° FWHM. Fermi surfaces were acquired by rotating the sample in polar and azimuthal directions to collect photocurrent spread uniformly over the hemisphere above the crystal surface. The resulting data sets are presented in a $\mathbf{k}_\parallel$ projection, where $\mathbf{k}_\parallel$ denotes the electron momentum parallel to the surface.

A home-made scanning tunnelling microscope operated at 8 K was used to study the conductance of individual $C_{60}$ molecules. Conductance-versus-displacement curves were acquired by approaching the tip towards the molecule at $\approx$45 Å $s^{-1}$ and simultaneously recording the current. Contact between the tip and the molecule was controllably performed and led to a reproducible contact conductance.

## 3. The Kohn effect

The Kohn effect manifests the collapse of the adiabatic or the Born–Oppenheimer approximation. In this approximation electrons are considered to respond instantaneously to the motions of the ions in a metal. The argument is that electrons are light in comparison and move rapidly. However, the electrons do not move infinitely fast and thus if an ion is displaced the electron system will for a short but finite time be in an excited state. Depending on the dimensionality of the system, this scenario may lead to the renormalization of electron and phonon dispersion relations. The Kohn effect describes anomalous phonon dispersion curves as a result of nonadiabatic coupling to the electron system.

To illustrate the effect we consider a one-dimensional free-electron gas coupled to a chain of ions with a given spatial periodicity. The phonon dispersion relation can be derived within mean-field theory to give [26]

$$\omega^2(q) = \omega_0^2(q) + 2\hbar^{-1} g^2 \omega_0(q) \chi(q, T), \tag{1}$$

where $q$ denotes the wavevector of the phonon, $g$ is the coupling strength between electrons and phonons, $\chi$ is Lindhard's dielectric function, $\hbar$ is Planck's constant, and the index 0 indicates the dispersion of the bare phonon. The Lindhard function describes the screening of an external charge by the conduction electrons. For vanishing temperature ($T$ = 0 K) and linear electron dispersion close to the Fermi energy $E_F$, it can be shown [1] that

$$\chi(q) \propto \ln\left(\frac{q + 2k_F}{q - 2k_F}\right), \tag{2}$$

where $k_F$ is the Fermi wavevector. Thus, external charge oscillations with critical wavevector $q_c = 2k_F$ lead to an electronic instability at the Fermi level. We notice that the derived result holds in the static approximation, i.e. for $\omega/(k_F v_F) \to 0$ (with $v_F$ the Fermi velocity). Beyond the static approximation, the singularity of $\chi(q)$ occurs at $q_c = 2k_F \pm \omega/v_F$ [27].

The divergent behaviour of $\chi(q)$ at $q_c = 2k_F$ can be related to the topology of the Fermi surface involved. The higher the number of electron states (one occupied, the other unoccupied) with energies close to $E_F$ and wavevectors differing by $2k_F$, the larger is the value of $\chi(q_c)$. For systems which exhibit one-dimensional character the Fermi surface consists of two parallel planes with distance $2k_F$ in reciprocal space. Consequently, there are infinitely many states with the above mentioned properties and hence $\chi(q)$ diverges at $q_c = 2k_F$. This situation is often referred to as perfect nesting of Fermi surface contours and the atomic chain undergoes the so-called Peierls transition. The latter describes a static distortion of the spatial periodicity of the monatomic chain [28]. The Fermi surface of a two-dimensional free-electron gas is a circle with diameter $2k_F$. For a given direction there is consequently only a single electron–hole pair satisfying the requirements and thus $\chi(q)$ is finite at $q_c = 2k_F$. Kohn predicted that phonon dispersion curves revealed kinks at $q_c = 2k_F$ which are due to the nonanalytic behaviour of

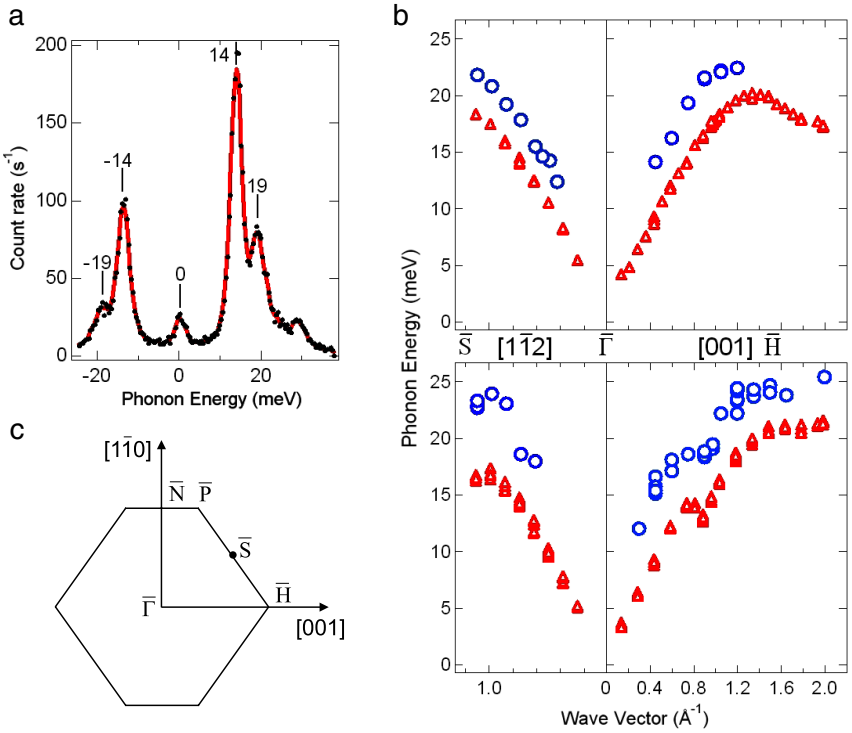


**Figure 1.** (a) Surface phonon spectrum of clean Mo(110) at room temperature. The energy of incident electrons was set to 25 eV. The analyser was rotated so as to measure electrons which transferred momentum of 0.75 Å$^{-1}$ to the sample. Spectroscopic signatures of the longitudinal and the transverse acoustic surface phonons are located at ±19 and ±14 meV, respectively. Positive (negative) energies correspond to an energy loss (energy gain) of the probing electrons. The peak at zero energy reflects quasi-elastically scattered electrons. (b) Surface phonon dispersion curves of the clean (top) and the hydrogen-saturated (bottom) Mo(110) surface at 110 K. Triangles and circles depict the dispersion curves of the transverse and longitudinal acoustic phonon modes, respectively. Indentations occur along [001] at ≈0.9 Å$^{-1}$ for both phonon modes, while along [1$\bar{1}$2] the energy of the transverse acoustic surface phonon is lowered at ≈1.2 Å$^{-1}$. (c) Sketch of the Mo(110) surface Brillouin zone.

$\chi(q)$ at $q_c$ [29]. Experimentally, these kinks were reported for lead and molybdenum bulk crystals using inelastic neutron scattering [30, 31] and thenceforward referred to as Kohn anomalies.

We notice that the Kohn anomaly may be characterized as a precursor state of the Peierls transition. While for the Kohn anomaly the phonons are dynamically softened which is revealed by small kinks in their dispersion curves, the Peierls transition describes a static lattice distortion for which the kinks in the phonon dispersion curves evolve into indentations to zero energy. For instance, a Kohn anomaly may turn into a Peierls distortion for sufficiently low temperatures.

For quasi-one-dimensional Fermi surface nesting the Kohn anomaly may lead to considerable indentations in the dispersion curve. Hulpke and Lüdecke showed by inelastic helium atom scattering (HAS) that the hydrogen-covered W(110) surface exhibits a Kohn anomaly of this type [32]. Later, other Kohn anomaly systems were analysed by HAS and EELS like the hydrogen- and deuterium-covered Mo(110) surface [33, 34] as well as the hydrogen-covered alloy $Mo_{1-x}Re_x(110)$ $(0 < x \leqslant 0.25)$ [35].

We restrict ourselves here to the discussion of the hydrogen-covered Mo(110) surface. HAS experiments on the hydrogen-saturated Mo(110)–(1 × 1)H surface reported two anomalous dispersion branches for the transverse acoustic (TA) surface phonon along [001] [33]. These branches showed indentations at a wavevector of ≈0.9 Å$^{-1}$ with different magnitudes. The phonon energy in the shallow indentation was ≈3 meV lower than observed for the clean surface, while the strong indentation showed an energy lowering of as much as ≈14 meV. As revealed by a subsequent EELS experiment on this adsorbate system, similar indentations of the dispersion curves were reported for the longitudinal acoustic (LA) surface phonon and at additional locations in the surface Brillouin zone [34]. Figure 1 summarizes a part of the results reported in [34]. A typical phonon spectrum is shown in figure 1(a). Energy loss and gain sides of the spectrum are given by positive and negative electron energies, respectively. Spectroscopic signatures of the TA and LA surface phonon modes are peaks located at ±14 and ±19 meV, respectively. Quasi-elastically scattered electrons are collected in the peak at zero energy. The spectrum presented in figure 1(a) was acquired with the spectrometer analyser rotated so as to detect electrons with a momentum transfer of 0.75 Å$^{-1}$. For the complete dispersion curves shown in figure 1(b) many phonon spectra were recorded at a variety of wavevectors along symmetry directions of the surface Brillouin zone (see figure 1(c)). While the clean Mo(110) surface exhibits normal dispersion curves of the TA and LA surface phonons along [001] and [1$\bar{1}$2] (see the top panel of figure 1(b)), the hydrogen-saturated surface shows

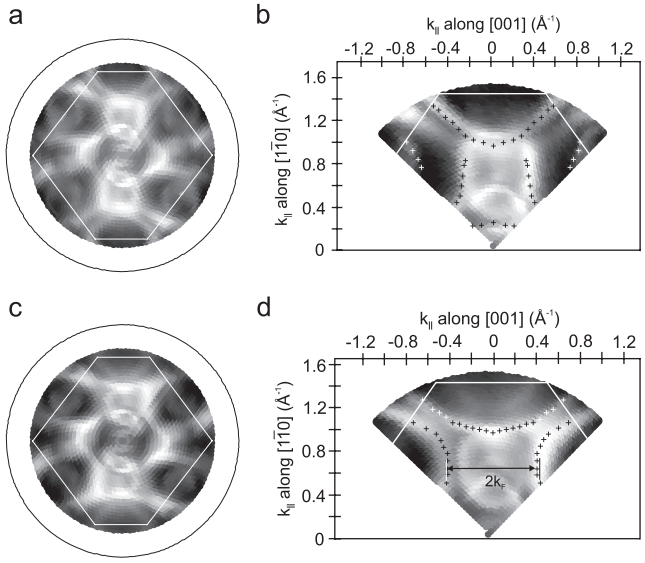


**Figure 2.** (a) Fermi surface of surface-localized states of clean Mo(110) acquired at room temperature. The photocurrent is displayed on a logarithmic scale. Dark (bright) areas correspond to low (high) photoelectron intensity. Thin white lines indicate the surface Brillouin zone boundary. (b) Close-up view of (a) showing the upper sector of the Fermi surface map. Calculated [37] data are included as crosses. (c) The same as (a) for hydrogen-saturated Mo(110). (d) The same as (b) for hydrogen-saturated Mo(110). The distance between nested contours of the Fermi surface is indicated as $2k_F$.

anomalous indentations for the TA and LA surface phonon dispersion along [001] at ≈0.9 Å$^{-1}$ and for the TA phonon mode along [1$\bar{1}$2] at ≈1.2 Å$^{-1}$.

To identify the nature of the anomalous softening of surface phonons an ARPES experiment was performed [36]. The key result of this experiment is presented in figure 2, where Fermi surfaces of the clean (top panel) and the hydrogen-saturated (bottom panel) Mo(110) surface are shown. Figures 2(a) and (c) show the complete Fermi surface covering more than the first surface Brillouin zone (indicated by white lines). In figures 2(b) and (d) we focus on a particular part of the surface Brillouin zone to reveal the changes in the Fermi surface topology clearly. To the latter Fermi surface maps we added calculated results as crosses [37]. According to these calculations the surface potential is modified upon hydrogen adsorption and gives rise to a shift of a $d_{3z^2-r^2,xy}$ band along the [001] direction into the (110) projected band gap of bulk electronic states. These d states therefore lose their three-dimensional character and turn into surface resonances and surface states. In addition, the Fermi surface contours of these states are nested. The corresponding theoretical nesting vectors are in good agreement with the critical wavevectors for softened surface phonons as reported by HAS [33] and EELS [34]. Moreover, as seen from figure 2(d), the calculated nesting vector is in accordance with the experimental nesting vector reported by ARPES [36]. Because of this agreement between theory and experiment and between HAS, EELS and ARPES, the anomalous softening of the acoustic surface phonons was interpreted as a Kohn anomaly due to quasi-one-dimensional Fermi surface nesting (see also table 1 for a comparison of critical wavevectors and nesting vectors). Nesting vectors $2k_F$ were extracted from Fermi surface maps by finding the maximum intensity at the Fermi level. This method is appropriate because the surface state bands involved have an occupied band width of 800 meV and the energy resolution of the spectrometer was set to 35 meV [36]. As a consequence, there is no need for more sophisticated methods to determine $k_F$. The latter become necessary if the occupied band width is of the same order as the instrumental energy resolution, as reported in detail in [38, 39].

**Table 1.** Comparison of critical wavevectors $q_c$ as obtained by HAS [33] and EELS [34] with nesting vectors $2k_F$ as reported by ARPES [36] and density functional theory (DFT) [37].

| Direction | $q_c^{HAS}$ (Å$^{-1}$) | $q_c^{EELS}$ (Å$^{-1}$) | $2k_F^{ARPES}$ (Å$^{-1}$) | $2k_F^{DFT}$ (Å$^{-1}$) |
|---|---|---|---|---|
| [001] | 0.89 | $0.90 \pm 0.03$ | $0.85 \pm 0.04$ | 0.86 |
| [1$\bar{1}$2] | — | $1.22 \pm 0.03$ | $1.19 \pm 0.04$ | 1.23 |

We close this section by mentioning a theoretical scenario put forward by Bungaro *et al* [40] to explain the anomalous softening of the transverse acoustic surface phonon on W(110)–(1 × 1)H [32, 41], which is similar to the one for Mo(110)–(1 × 1)H. Interestingly, without any essential approximation other than the adiabatic one, Bungaro and co-workers obtained the full surface phonon dispersion curve. As a consequence, they were able to model the shallow dip without any electron–phonon coupling. They consistently concluded that the observed phonon anomaly was not of the Kohn type. Instead, Bungaro *et al* suggested that the anomalous branch could correspond to a collective plasmon-like mode of the hydrogen adsorption layer. However, in the light of the good agreement between results of HAS [32], EELS [41], ARPES [42] and theory [37] concerning critical wavevectors of softened phonons and nesting vectors of Fermi surface contours, the anomalous phonon dispersion on W(110)–(1 × 1)H is most probably caused by the Kohn effect.

## 4. Nonadiabatic electronic damping of adsorbate vibrations

The damping of vibrational modes due to electron–hole pair creation is another manifestation of electron–phonon coupling at surfaces [43–47]. Time-resolved laser experiments on, for instance, Cu(100)–CO [48, 49] and Cu(111)–CO [50] were able to resolve the electron and phonon contribution to the adsorbate–substrate coupling. Vibrational modes of adsorbates reveal an infinite lifetime in the adiabatic and harmonic approximation. A finite lifetime, however, is observed because of the collapse of one of these simplifications. For instance, anharmonic effects couple vibrations to other modes of the system such as the substrate phonons. Since typical adsorbate–substrate or intermolecular vibrational energies are much higher than phonon energies, adsorbate vibrations can decay only by the simultaneous creation of many phonons. This is a rather improbable event unless the anharmonicity is very large.

A failure of the Born–Oppenheimer approximation likewise can lead to the decay of a vibrational mode as discussed below.

The physical picture behind the electronic damping of an adsorbate vibration is provided by the following simplified discussion. Consider a single electron level of an atomic adsorbate. This level contributes to the electronic density of states at the Fermi level of the hosting substrate. According to Lang and Williams [51] the adsorbate level rises and falls as the adsorbate vibrates back and forth. If the atom motion is sufficiently slow electrons flow in and out of the level to maintain a common Fermi level with the substrate. For faster motion of the adsorbate the electrons lag behind and states which should be occupied in the adiabatic ground state remain empty. Consequently, an electron–hole pair appears in the induced density of states. In other words, energy has been transferred from the vibrating atom to the substrate electronic system; i.e., the adsorbate vibration is damped, reflecting a breakdown of adiabaticity of the order of $\omega_r\tau$. The asymmetry parameter $\omega_r\tau$ contains the renormalized vibrational frequency $\omega_r$ and the damping rate $\tau^{-1}$. The electron–hole damping of the adsorbate vibration is thus explained in terms of an enhanced coupling of the discrete vibrational excitation to the electron continuum of the substrate [52]. Langreth [52] showed that the line shape of vibrational modes may give unambiguous evidence of whether electron–hole pair production is an effective energy transfer mechanism in the electron–vibration coupling. It was further shown [52] that an inescapable consequence of the electron–hole damping is an asymmetric line shape in the spectrum of the vibrational mode, which couples nonadiabatically to the electronic continuum. The asymmetry increases with increasing nonadiabatic effects. The analytic expression for the line shape reads [52]

$$L(\omega) = c\gamma\omega_r\omega\frac{\left[1-\frac{\tau}{\gamma}\left(\omega^2-\omega_r^2\right)\right]^2}{\left(\omega^2-\omega_r^2\right)^2+\gamma^2\omega^2}, \qquad (3)$$

where $c$ is a constant containing the dynamic dipole moment of the adsorbate and $\gamma$ denotes the FWHM of the line shape.

The first experiment hinting at this kind of coupling was carried out by infrared reflection absorption spectroscopy (IRAS) on W(100)–H and W(100)–D [53]. The spectroscopic signature of the hydrogen and deuterium wagging mode exhibited an extraordinarily asymmetric line shape while the symmetric stretch modes did not show this asymmetry. The electronic continuum which is responsible for the damping of the H and D wagging modes was identified by reflectivity measurements [54]. According to these measurements an electronic surface state with $d_{xy}$ character was proposed. Using EELS, evidence for electron–hole damping was reported for Mo(110)–H, Mo(110)–D [34], Mo(110)–Li [55], and for the metal–organic interface Ag(111)–PTCDA (3,4,9,10-perylene-tetracarboxylic acid-dianhydride) [56].

In figure 3 we show an example of nonadiabatic damping of an adsorbate vibration mode. Here, a specular electron energy loss spectrum of Mo(110)–(1 × 1)D is presented. The (1 × 1) superstructure corresponds to the deuterium saturation coverage. While the peaks at ≈73 and ≈113 meV correspond to D vibrational modes parallel and perpendicular to the surface

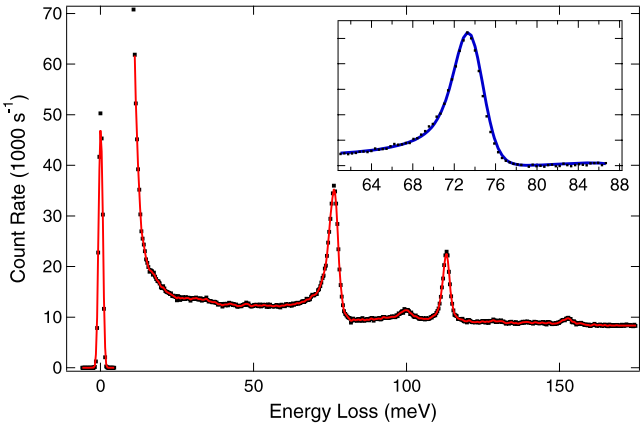


**Figure 3.** Specular spectrum of Mo(110)–(1 × 1)D acquired with an electron impact energy of 5 eV. The peak at zero energy represents elastically scattered electrons; the peaks at ≈73 meV and at ≈113 meV are the signatures of parallel and perpendicular deuterium vibration modes, respectively. The loss spectrum was multiplied by a factor of five to share a common axis with the zero energy peak. The small features around 100 and 152 meV are caused by hydrogen vibrations. Inset: close-up view of the line shape of the parallel deuterium vibration mode after subtraction of a linear background matching the tail of the elastic peak.

respectively, the small peaks at ≈100 and ≈152 meV are the spectroscopic signatures of hydrogen vibrations. In the inset of figure 3 a close-up view of the line shape of the parallel deuterium vibration mode is shown. The full line depicts the result of fitting experimental data by the line shape according to equation (3) convoluted with a Gaussian reflecting a spectrometer energy resolution of 1.5 meV. Prior to fitting, a linear background was subtracted matching the tail of the elastic peak.

In table 2 fit parameters for several systems are compared. From this comparison we can infer that, first, the strength of the interaction between the adsorbate vibration and the electronic system of the substrate as monitored by $\omega_r\tau$ does not depend strongly on the temperature (first five rows of table 2). While the width of the line shape increases upon increasing the temperature, its asymmetry remains nearly the same. Second, the dependence of the asymmetry parameter on isotopes (H and D) is negligible. This is expected since isotopes are chemically identical and thus do not modify the substrate's electronic structure in a different way. Reutt *et al* [54] showed in this context that the asymmetry of the line shape is modified substantially when small amounts of CO are coadsorbed on Mo(100)–H. This observation was attributed to a significant CO-induced modification of the electronic structure of the substrate.

We close this section by addressing the question of why vibrational modes with a certain polarization are damped, for instance the H wagging modes on W(100) and Mo(100) or the parallel H and D modes on Mo(110), while others are not affected by nonadiabatic damping, e.g. the symmetric stretch modes of H on W(100) or Mo(100) or the perpendicular D vibration on Mo(110) (see the Lorentzian line shape of the D vibration mode at 152 meV in figure 3). The current interpretation is based on a symmetry requirement for the

**Table 2.** Comparison of renormalized frequencies ($\omega_r$), line widths ($\gamma$) and asymmetry parameters ($\omega_r\tau$) of hydrogen, deuterium and lithium vibration modes on various surfaces.

| Surface | Mode | $T$ (K) | $\omega_r$ (meV) | $\gamma$ (meV) | $\omega_r\tau$ | Reference |
|---|---|---|---|---|---|---|
| Mo(100)-(1 × 1)H | Wagging | 100 | 161.4 | 1.5 | 0.37 | [54] |
| | | 245 | 161.2 | 2.2 | 0.40 | [54] |
| W(100)-(1 × 1)H | Wagging | 100 | 157.7 | 2.3 | 0.54 | [54] |
| | | 300 | 157.3 | 2.7 | 0.53 | [54] |
| W(100)-(1 × 1)D | Wagging | 300 | 113.9 | 3.1 | 0.5 | [54] |
| Mo(110)–(1 × 1)H | Parallel | 110 | 99.9 | 4.3 | 0.19 | [34] |
| Mo(110)–(1 × 1)D | Parallel | 110 | 73.8 | 2.0 | 0.20 | [34] |
| W(110)–(1 × 1)H | Parallel | 110 | 100.9 | 17.9 | 0.74 | [34] |
| Mo(110)–Li | Perpendicular | 110 | 38.7 | 1.6 | 0.16 | [55] |

electronic states which are involved in the damping. For a vibration mode which is even (odd) with respect to a mirror plane of the surface, the product of the initial and final electronic state must be even (odd). Smith *et al* [57] found an adsorbate-induced electronic surface state on W(100)–H which provides the correct symmetry for an efficient damping. For H, D, or Li on Mo(110) a similar scenario may be responsible for the damping. However, a corresponding study is still lacking. Interestingly, the parallel hydrogen vibration mode on Mo(110) exhibits a Kohn-anomaly-like dispersion curve while the perpendicular mode disperses weakly [58].

## 5. Conductance and local heating of a single molecule

In this paragraph we introduce a scanning tunnelling microscopy (STM) experiment in which the tip of the microscope is controllably and reproducibly brought into contact with an individual $C_{60}$ molecule adsorbed on Cu(100). Contact between the tip and the molecule is accompanied by an electric current of $\approx$10 $\mu$A which is ballistically transferred through the molecule. This situation leads to heating of the molecule up to effective temperatures which are considerably higher than the cryogenic environment the experiments are performed in. Local heating occurs when electrons diffusing in a conductor release energy to the ions via scattering with phonons. The amount of heat generated in a given portion of the conductor depends on the electron–phonon interaction, the current density, the background temperature, and the inelastic electron mean free path. In a nanoscale junction, the inelastic electron mean free path is large compared to the dimensions of the junction. Consequently, each ballistically transferred electron releases only a small fraction of its energy on its way through the constriction [59, 60]. However, there can still be substantial local heating due to the large current density. Such an effect has been observed in several atomic-scale structures [61–67]. For instance, experiments using metal nanobridges or the mechanically controlled break junction technique report on time series of two-level resistance fluctuations of the constriction between the electrodes. From their experiments, Ralls *et al* [62, 63] concluded that the two-level fluctuations in the resistance originate from reversible motion of an atomic-scale defect in the constriction region between two metastable states. Recently, using conducting atomic force microscopy, Huang *et al* [68] reported on current-induced local heating of a single molecule. Here, we show evidence of local heating of an individual $C_{60}$ molecule in contact with the tip of a scanning tunnelling microscope.

Electronic and mechanical properties of materials at the nanometre scale differ from those of macroscopic materials. For instance, electron transport through constrictions whose width is comparable with the electron wavelength is quantized. According to Landauer [69], the conductance $G = I/V$ (where $I$ denotes the current and $V$ the voltage) is expressed as

$$G = G_0 \sum_n \tau_n, \tag{4}$$

where $\tau_n$ is the transmission probability of the $n$th transport channel and $G_0 = 2e^2/h$ the quantum of conductance ($e$, electron charge; $h$, Planck's constant). We notice that the Landauer conductance introduced in equation (4) arises from elastic transmission and is not associated with any dissipation in the junction. It has been shown by the mechanically controlled break junction technique that the number of transport channels in a one-atom contact is mainly determined by the number of valence orbitals of the atom, and the transmission probability of each channel is fixed by the local atomic environment [70, 71].

Scanning probe techniques have been used to form contacts between the tip and a metal surface whose quantized conductance was then investigated during forming and stretching of the constriction [72–74]. Microscopic control of this kind of experiment was added by experiments where the contact area was imaged prior to and after contact. For instance, flat surfaces as well as individual silver adatoms on Ag(111) and single copper adatoms on Cu(111) were contacted controllably and reproducibly by the tip of a scanning tunnelling microscope [75]. Analogous results were obtained for cobalt adatoms on Cu(100) [76] and gold atoms on Au(111) [77]. Contact measurements on molecules using the scanning tunnelling microscope are, however, scarce. A pioneering experiment was performed by Joachim *et al* [78] to study the contact conductance of $C_{60}$ on Au(110) at room temperature. Néel *et al* [79, 80] investigated Cu(100)–$C_{60}$ with a low-temperature scanning tunnelling microscope. The results of this experiment are reviewed in this section.

Figure 4(a) shows a constant-current STM image of Cu(100)–$C_{60}$ in the submonolayer coverage regime. The bright and dim rows correspond to chains of $C_{60}$ molecules along the indicated crystallographic directions. By combining STM and x-ray photoelectron diffraction data Abel *et al* [81]

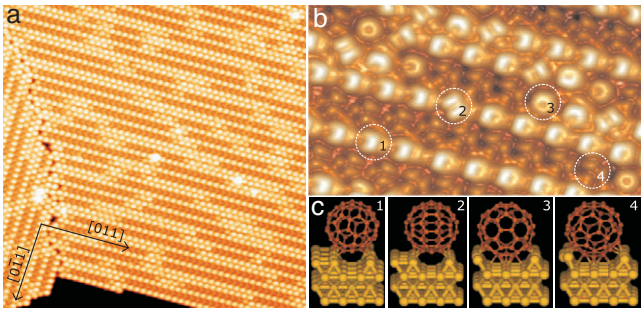


**Figure 4.** (a) STM image of a $C_{60}$ island adsorbed on Cu(100) ($V = 1.5$ V, $I = 1$ nA, 400 Å × 400 Å). Molecule chains appear as bright and dim rows due to adsorption-induced surface reconstruction. (b) Close-up view of (a) showing individual $C_{60}$ molecules with intramolecular resolution (130 Å × 75 Å). (c) Molecule orientations on missing-row-reconstructed Cu(100) (courtesy of Th Frederiksen, University of Denmark). The numbers refer to the molecules encircled by a dashed line in (b). Image processing was performed by Nanotec WSxM [82].

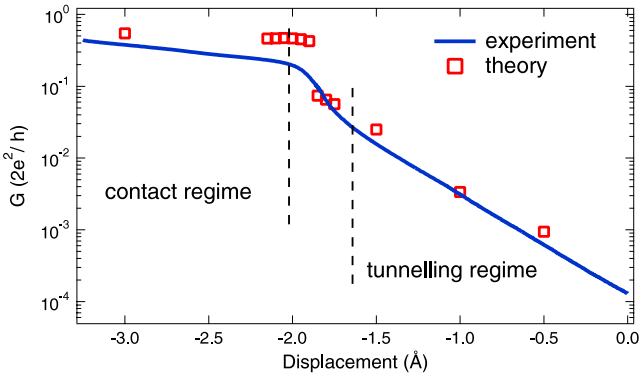


**Figure 5.** Conductance versus displacement for a $C_{60}$ molecule denoted as 1 in figure 4(b). The conductance is plotted on a logarithmic scale and in units of $G_0$. Owing to the high number of data points experimental data appear as a line. Calculated data are depicted as squares. Zero displacement corresponds to a tip–molecule distance defined by feedback loop parameters of 0.3 V and 3 nA.

concluded that these stripe patterns were due to a $C_{60}$-induced missing row reconstruction of the underlying substrate surface. The close-up view in figure 4(b) displays individual $C_{60}$ molecules within the bright and dim stripes with submolecular resolution. We attribute the intramolecular structure to the spatial distribution of the second-to-lowest unoccupied molecular orbital in agreement with [83]. Lu *et al* [83] combined STM data and *ab initio* pseudopotential density functional calculations to explain the spatial inhomogeneous $C_{60}$ local electronic structure on Ag(100). Figure 4(c) identifies the adsorption geometry of $C_{60}$ molecules encircled by a dashed line in figure 4(b). Molecules 1 and 2 adsorb on Cu rows which embrace a single missing Cu row, while molecules 3 and 4 occupy substrate atomic rows which embrace two missing rows. The orientation of each molecule differs; i.e., molecule 1 exhibits a C–C bond between a carbon pentagon and a carbon hexagon at the top, molecule 2 shows a C–C bond between two adjacent carbon hexagons, and molecules 3 and 4 exhibit a pentagon and a hexagon at the top, respectively. In the following we focus the discussion on molecule 1.

How does the conductance of an individual molecule change with decreasing distance between the tip and the molecule? Figure 5 shows a conductance curve acquired on molecule 1 with the tip approaching the molecule at ≈45 Å $s^{-1}$. The displacement ($\Delta z$) describes the extension of the piezo tube hosting the tip; i.e., the more negative the displacement the smaller is the tip–molecule distance. The conductance curves may be divided into three parts which are characterized by different slopes. Between $\Delta z = 0$ and $\Delta z \approx -1.6$ Å the conductance varies exponentially from $10^{-4}G_0$ to $\approx 0.025G_0$ as expected from the exponential dependence of a tunnelling current on the tip–surface distance. We therefore call this part of the conductance curve the tunnelling regime. Starting from $\Delta z \approx -1.6$ Å we observe deviations from the exponential behaviour. A sharp increase of the conductance by a factor of 10 to $\approx 0.25G_0$ occurs within a displacement interval of only ≈0.4 Å. Further decrease of the tip–molecule distance increases the conductance slowly. Figure 5 contains calculated data depicted as squares. Calculations were performed using SIESTA [84] and TRANSIESTA [85] density functional theory packages. A detailed description of the applied model can be found in [76]. The most intriguing observation is that theory is able to model the sharp increase of the conductance and the contact conductance, which is as low as $\approx 0.25G_0$. The conductance of single-adatom contacts [75, 77, 79] was given by approximately a quantum of conductance. The rapid rise of the conductance in the displacement interval between ≈−1.6 Å and ≈−2.0 Å can be understood from the relaxed tip–molecule geometries which the model calculations are based on. As the electrode separation is reduced by only 0.05 Å, the tip–molecule distance shrinks by 0.84 Å. This strong reduction of the tip–molecule distance corresponds to the formation of a bond between the tip apex and the $C_{60}$, which hence effectively closes the tunnelling gap. In this transition regime between tunnelling and contact only small energy differences discriminate between the configurations with or without the tip–molecule bond. At finite voltages and under nonequilibrium conditions imposed by the bias voltage it is thus likely that the junction will fluctuate between these different configurations. With $G_t$ and $G_c$ the conductances just before and just after contact, respectively, a thermally averaged conductance can be calculated according to

$$\bar{G}(\Delta z) = \frac{G_t(\Delta z)\exp(-\beta E_t(\Delta z)) + G_c(\Delta z)\exp(-\beta E_c(\Delta z))}{\exp(-\beta E_t(\Delta z)) + \exp(-\beta E_t(\Delta z))} \quad (5)$$

with $\beta = (k_B T)^{-1}$ and $k_B$ Boltzmann's constant. $E_t$ and $E_c$ denote the total energies of a tunnelling and a contact configuration, respectively.

In figure 6 we focus on the conductance curve in a displacement interval around the instability point. Increasing the effective temperature of the tip–molecule junction from 0 K (squares) via 8 K (thin dashed line) up to 400 K (thick dashed line) leads, first, to an increase of the width of the

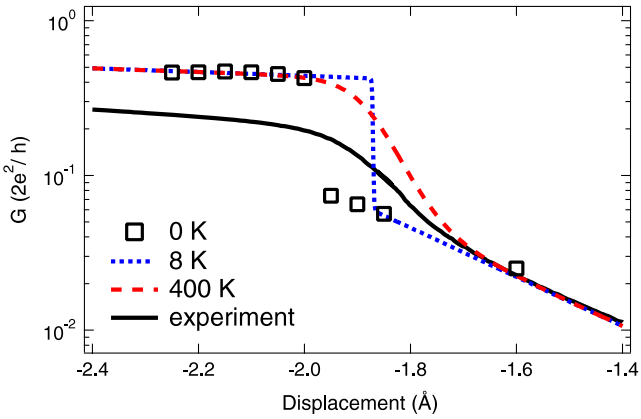


**Figure 6.** Width of the transition regime dependent on the effective temperature of the junction. Experimental data appear as a line while calculated data are depicted as squares for $T_{\text{eff}} = 0$ K, as a thin dashed line for $T_{\text{eff}} = 8$ K, and as a thick dashed line for $T_{\text{eff}} = 400$ K.

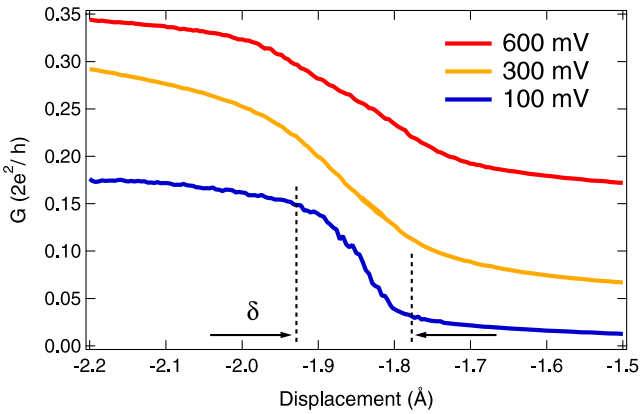


**Figure 7.** Comparison of conductance curves acquired at indicated voltages. The width, $\delta$, of the displacement interval for the transition is shown for the curve taken at 100 mV. Conductance curves at 300 and 600 mV are vertically offset.

**Table 3.** Widths of the transition interval ($\delta$) and effective temperatures ($T_{\text{eff}}$) for conductance curves acquired at different voltages ($V$).

| $V$ (mV) | $\delta$ (Å) | $T_{\text{eff}}$ (K) |
|---|---|---|
| 100 | 0.2 | 300 |
| 300 | 0.4 | 400 |
| 600 | 0.5 | 700 |

conductance curve and, second, to a shift of the instability displacement to more positive values of the displacement. At an effective temperature of 400 K the width of the calculated conductance curve matches well the width of the experimental curve. Because of this elevated temperature we propose a scenario of local heating of the molecule in contact with the tip. This suggestion is further corroborated by the experimental observation that the width of the displacement interval of the transition regime increases with increasing voltage as shown in figure 7. In table 3 we compare the widths and the corresponding effective temperatures.

The dependence of the effective temperature on the voltage was modelled for atom-sized contacts by assuming a bulk thermal conduction mechanism [59, 86, 87]. From these investigations it follows that the effective temperature for small ambient temperatures is proportional to the square root of the voltage. However, there are examples where the effective temperature rises more rapidly than $\sqrt{V}$, for instance, the bias-induced local heating of Zn atom-sized contacts [88]. For octanedithiol the $\sqrt{V}$ law for the effective temperature seems to approximately hold [68], while in our case of $C_{60}$ more experimental data and theoretical analysis would be needed to estimate the voltage dependence of the effective temperature.

## 6. Summary

The interaction between phonons and electrons was discussed in terms of the Kohn effect, nonadiabatic damping of adsorbate vibration modes, and the local heating of a single molecule.

To unambiguously identify an anomalous softening of phonons as the Kohn effect, the combination of results obtained by vibrational spectroscopies and photoemission experiments is useful. Along this line, the hydrogen-covered Mo(110) surface was shown to be a Kohn anomaly system owing to quasi-one-dimensional nesting of Fermi surface contours.

Adsorbate vibrations may be damped by creation of electron–hole pairs. This process leaves its fingerprint as an asymmetric line shape in vibrational spectra of the damped vibration mode. The rate of energy transfer between the discrete vibration and the continuum of electron–hole pairs can be inferred from an analysis of the line shape.

Molecules can be controllably contacted by the tip of a scanning tunnelling microscope without either deteriorating the imaging capability of the tip or destroying the contact area. The contact conductance of specifically addressed molecular orbitals can thus be studied. In the transition between tunnelling and contact the molecule fluctuates between tunnelling and contact configurations with the tip.

## Acknowledgments

The results of the presented work were obtained with the strong and fruitful cooperation of other scientists. I am delighted to thank S Lehwald and H Ibach (Research Centre Julich, Germany), Th Greber and J Osterwalder (University of Zurich, Switzerland), Th Frederiksen and M Brandbyge (University of Denmark, Denmark), and N Néel, L Limot, and R Berndt (University of Kiel, Germany).

## References

[1] Ashcroft N W and Mermin N D 1976 *Solid State Physics* (Philadelphia, PA: Saunders College Publishing)
[2] Grimvall G 1981 *The Electron–Phonon Interaction in Metals* (*Series of Monographs on Selected Topics in Solid State Physics*) (Amsterdam: North-Holland)
[3] Bardeen J, Cooper N L and Schrieffer J R 1957 *Phys. Rev.* **108** 1175
[4] Matzdorf R, Meister G and Goldmann A 1993 *Surf. Sci.* **286** 56
[5] McDougall B A, Balasubramanian T and Jensen E 1995 *Phys. Rev.* B **51** 13891

[6] Matzdorf R, Meister G and Goldmann A 1996 *Phys. Rev.* B **54** 14807
[7] Balasubramanian T, Jensen E, Wu X L and Hulbert S L 1998 *Phys. Rev.* B **57** R6866
[8] Hofmann Ph, Cai Y Q, Grütter Ch and Bilgram J H 1998 *Phys. Rev. Lett.* **81** 1670
[9] Valla T, Fedorov A V, Johnson P D and Hulbert S L 1999 *Phys. Rev. Lett.* **83** 2085
[10] Straube P, Pforte F, Michalke T, Berge K, Gerlach A and Goldmann A 2000 *Phys. Rev.* B **61** 14072
[11] Balasubramanian T, Glans P A and Johansson L I 2000 *Phys. Rev.* B **61** 12709
[12] Eiguren A, Hellsing B, Reinert F, Nicolay G, Chulkov E V, Silkin V M S, Hüfner S and Echenique P M 2002 *Phys. Rev. Lett.* **88** 066805
[13] Tang S J, Ismail, Sprunger P T and Plummer E W 2002 *Phys. Rev.* B **65** 235428
[14] Gayone J E, Kirkegaard C, Wells J W, Hoffmann S V, Li Z and Hofmann Ph 2005 *Appl. Phys.* A **80** 943
[15] Hengsberger M, Purdie D, Segovia P, Garnier M and Baer Y 1999 *Phys. Rev. Lett.* **83** 592
[16] Hengsberger M, Frésard R, Purdie D, Segovia P and Baer Y 1999 *Phys. Rev.* B **60** 10796
[17] LaShell S, Jensen E and Balasubramanian T 2000 *Phys. Rev.* B **61** 2371
[18] Ast C R and Höchst H 2002 *Phys. Rev.* B **66** 125103
[19] Shi J, Tang S J, Wu B, Sprunger P T, Yang W L, Brouet V, Zhou X J, Hussain Z, Shen Z X, Zhang Z and Plummer E W 2004 *Phys. Rev. Lett.* **92** 186401
[20] Kröger J, Lehwald S and Ibach H 2004 *Phys. Rev.* B **69** 201404
[21] Kröger J 2006 *Rep. Prog. Phys.* **69** 899
[22] Hellsing B, Eiguren A and Chulkov E V 2002 *J. Phys.: Condens. Matter* **14** 5959
[23] Echenqiue P M, Berndt R, Chulkov E V, Fauster Th, Goldmann A and Höfer U 2004 *Surf. Sci. Rep.* **52** 219
[24] Ibach H 1993 *J. Electron Spectrosc. Relat. Phenom.* **64-65** 819
[25] Greber T, Raetzo O, Kreutz T J, Schwaller P, Deichmann W, Wetli E and Osterwalder J 1997 *Rev. Sci. Instrum.* **68** 4549
[26] Grüner G 2000 *Density Waves in Solids* (Cambridge: Perseus)
[27] Flatté M F 1994 *Phys. Rev.* B **50** 1190
[28] Peierls R P 1955 *Quantum Theory of Solids* (London: Oxford University Press)
[29] Kohn W 1959 *Phys. Rev. Lett.* **2** 393
[30] Brockhouse B N, Rao K R and Woods A D B 1961 *Phys. Rev. Lett.* **7** 93
[31] Powell B M, Martel P and Woods A D B 1968 *Phys. Rev.* **171** 727
[32] Hulpke E and Lüdecke J 1992 *Phys. Rev. Lett.* **68** 2846
[33] Hulpke E and Lüdecke J 1993 *Surf. Sci.* **287** 837
[34] Kröger J, Lehwald S and Ibach H 1997 *Phys. Rev.* B **55** 10895
[35] Okada M, Flach B, Hulpke E, Steinhögl W and Plummer E W 2002 *Surf. Sci.* **498** L78
[36] Kröger J, Greber T and Osterwalder J 2000 *Phys. Rev.* B **61** 14146
[37] Kohler B, Ruggerone P, Wilke S and Scheffler M 1995 *Phys. Rev. Lett.* **74** 1387
[38] Straub Th, Claessen R, Steiner P, Hüfner S, Eyert V, Friemelt K and Bucher E 1997 *Phys. Rev.* B **55** 13473
[39] Kipp L, Roßnagel K, Solterbeck C, Strasser T, Schattke W and Skibowski M 1999 *Phys. Rev. Lett.* **83** 5551
[40] Bungaro C, de Gironcoli S and Baroni S 1996 *Phys. Rev. Lett.* **77** 2491
[41] Balden M, Lehwald S and Ibach H 1996 *Phys. Rev.* B **53** 7479
[42] Rotenberg E and Kevan S D 1998 *Phys. Rev. Lett.* **80** 2905
[43] Persson M and Hellsing B 1982 *Phys. Rev. Lett.* **49** 662
[44] Persson B N J and Ryberg R 1985 *Phys. Rev.* B **32** 3586
[45] Naumovets A G and Vedula Y S 1985 *Surf. Sci. Rep.* **4** 365
[46] Zhang Z Y and Langreth D C 1989 *Phys. Rev.* B **39** 10028
[47] Tully J C, Gomez M and Head-Gordon M 1993 *J. Vac. Sci. Technol.* A **11** 1914
[48] Germer T A, Stephenson J C, Heilweil E J and Cavanagh R R 1993 *Phys. Rev. Lett.* **71** 3327
[49] Germer T A, Stephenson J C, Heilweil E J and Cavanagh R R 1994 *J. Chem. Phys.* **101** 1704
[50] Culver J P, Li M, Jahn L G, Hochstrasser R M and Yodh A G 1993 *Chem. Phys. Lett.* **214** 431
[51] Lang N D and Williams A R 1978 *Phys. Rev.* B **18** 616
[52] Langreth D C 1985 *Phys. Rev. Lett.* **54** 126
[53] Chabal Y J 1985 *Phys. Rev. Lett.* **55** 845
[54] Reutt J E, Chabal Y J and Christman S B 1988 *Phys. Rev.* B **38** 3112
[55] Kröger J, Bruchmann D, Lehwald S and Ibach H 2000 *Surf. Sci.* **449** 227
[56] Tautz F S, Eremtchenko M, Schaefer J A, Sokolowski M, Shklover V and Umbach E 2002 *Phys. Rev.* B **65** 125405
[57] Smith K E and Kevan S D 1989 *Phys. Rev. Lett.* **64** 567
[58] Kröger J, Lehwald S, Balden M and Ibach H 2002 *Phys. Rev.* B **66** 073414
[59] Todorov T N 1998 *Phil. Mag.* B **77** 965
[60] Montgomery M J, Todorov T N and Sutton A P 2002 *J. Phys.: Condens. Matter* **14** 5377
[61] van Gelder A P, Jansen A G M and Wyder P 1980 *Phys. Rev.* B **22** 1515
[62] Ralls K S and Buhrman R A 1988 *Phys. Rev. Lett.* **60** 2434
[63] Ralls K S, Ralph D C and Buhrman R A 1989 *Phys. Rev.* B **40** 11561
[64] Holweg P A M, Caro J, Verbruggen A H and Radelaar S 1992 *Phys. Rev.* B **45** 9311
[65] Muller C J, van Ruitenbeek J M and de Jongh J L 1992 *Phys. Rev. Lett.* **69** 140
[66] Persson B N J and Avouris P 1997 *Surf. Sci.* **390** 45
[67] Agraït N, Untiedt C, Rubio-Bollinger G and Vieira S 2002 *Phys. Rev. Lett.* **88** 216803
[68] Huang Z, Xu B, Chen Y, Ventra M D and Tao N 2006 *Nano Lett.* **6** 1240
[69] Landauer R 1970 *Phil. Mag.* **21** 863
[70] Cuevas J C, Yeyati A L and Martín-Rodero A 1998 *Phys. Rev. Lett.* **80** 1066
[71] Scheer E, Agraït N, Cuevas J C, Yeyati A L, Ludoph B, Martín-Rodero A, Rubio G, van Ruitenbeek J M and Urbina C 1998 *Nature* **394** 154
[72] Gimzewski J K and Möller R 1987 *Phys. Rev.* B **36** 1284
[73] Pascual J I, Méndez J, Gómez-Herrero J, Baró A M, García N and Binh V T 1993 *Phys. Rev. Lett.* **71** 1852
[74] Olesen L, Lægsgaard E, Stensgaard I, Besenbacher F, Schiøtz J, Stoltze P, Jacobsen K W and Nørskov J K 1994 *Phys. Rev. Lett.* **72** 2251
[75] Limot L, Kröger J, Berndt R, Garcia-Lekue A and Hofer W A 2005 *Phys. Rev. Lett.* **94** 126102
[76] Néel N, Kröger J, Limot L, Palotas K, Hofer W A and Berndt R 2007 *Phys. Rev. Lett.* **98** 016801
[77] Kröger J, Jensen H and Berndt R 2007 *New J. Phys.* **9** 153
[78] Joachim C, Gimzewski J K, Schlittler R R and Chavy C 1995 *Phys. Rev. Lett.* **74** 2102
[79] Néel N, Kröger J, Limot L, Frederiksen Th, Brandbyge M and Berndt R 2007 *Phys. Rev. Lett.* **98** 065502
[80] Néel N, Kröger J, Limot L and Berndt R 2007 *Nanotechnology* **18** 044027
[81] Abel M, Dmitriev A, Fasel R, Liu N, Barth J V and Kern K 2003 *Phys. Rev.* B **67** 245407
[82] Horcas I, Fernández R, Gómez-Rodríguez J M, Colchero J, Gómez-Herrero J and Baro A M 2007 *Rev. Sci. Instrum.* **78** 013705
[83] Lu X, Grobis M, Khoo K H, Louie S G and Crommie M F 2003 *Phys. Rev. Lett.* **90** 096802
[84] Soler J M, Artacho E, Gale J D, García A, Junquera J, Ordejón P and Sánchez-Portal D 2002 *J. Phys.: Condens. Matter* **14** 2745
[85] Brandbyge M, Mozos J L, Ordejón P, Taylor J and Stokbro K 2002 *Phys. Rev.* B **65** 165401
[86] Todorov T N, Hoekstra J and Sutton A P 2001 *Phys. Rev. Lett.* **86** 3606
[87] Chen Y C, Zwolak M and Ventra M D 2003 *Nano Lett.* **3** 1691
[88] Tsutsui M, Kurokawa S and Sakai A 2007 *Appl. Phys. Lett.* **90** 133121